Substrate interactions with suspended and supported monolayer MoS_{2}: Angle-resolved photoemission spectroscopy

Wencan Jin, Po-Chun Yeh, Nader Zaki, Datong Zhang, Jonathan T. Liou, Jerzy T. Sadowski, Alexey Barinov, Mikhail Yablonskikh, Jerry I. Dadap, Peter Sutter, Irving P. Herman, and Richard M. Osgood, Jr.

Substrate Interactions with Suspended and Supported Monolayer MoS2: Angle-Resolved Photoemission Spectroscopy

Wencan Jin,[1] Po-Chun Yeh,[1] Nader Zaki,[1] Datong Zhang,[1] Jonathan T. Liou,[1]
Jerry I. Dadap,[1] Irving P. Herman,[1] and Richard M. Osgood, Jr.[1,*]
[1] Columbia University, New York, New York 10027, USA

Jerzy T. Sadowski,[2] Peter Sutter[2]
[2] Center for Functional Nanomaterials, Brookhaven National Laboratory, Upton, New York 11973, USA

Alexey Barinov,[3] Mikhail Yablonskikh[3]
[3] Elettra Sincrotrone Trieste S.C.p.A., I-34012, Basovizza, Trieste, Italy

Abstract

We report the directly measured electronic structure of exfoliated monolayer molybdenum disulfide (MoS2) using micrometer-scale angle-resolved photoemission spectroscopy. Measurements of both suspended and supported monolayer MoS2 elucidate the effects of interaction with a substrate. A suggested relaxation of the in-plane lattice constant is found for both suspended and supported monolayer MoS2 crystals. For suspended MoS2, a careful investigation of the measured uppermost valence band gives an effective mass at $\bar{\Gamma}$ and $\bar{K}$ of $2.00m_0$ and $0.43m_0$, respectively. We also measure an increase in the band linewidth from the midpoint of $\overline{\Gamma K}$ to the vicinity of $\bar{K}$ and briefly discuss its possible origin.

Two-dimensional (2D) crystals of monolayer transition metal dichalcogenides (TMD) are of increasing interest both for their unusual physics and for their potential use in novel nanoelectronic devices [1, 2]. In particular, their substantial intrinsic bandgap of 1.3-1.9eV [3], which is thickness dependent, makes them a promising alternative to the most well studied 2D material, graphene, which lacks an intrinsic bandgap. Several fabrication techniques, including micromechanical exfoliation, chemical vapor deposition, and molecular beam epitaxy have been used to produce atomically thin TMD sheets on a variety of substrates. However, the substrate and any adsorbates may affect the electronic structure of TMD crystals and films via a modification of their dielectric environment or by the introduction of short- or long-range disorder. The latter is caused by chemical bonding or surface roughness. Particularly, in their monolayer form, interactions with a supporting substrate or adsorbed impurities are also known to influence the electronic structure [4] and significantly affect the electrical performance of Van der Waals materials [5, 6]. In addition, it has been shown that the substrate dielectric constant plays an important role in determining the excitonic binding energy as well as quasiparticle lifetime in 2D layered materials [7, 8]. Such phenomena thus make understanding of the effects of the substrate on 2D materials of pressing importance for both fundamental studies and potential applications in devices.

In order to minimize the effect of substrate interactions on atomically thin crystals, one of two different ameliorating procedures is typically utilized. One approach is to decouple the sample from the substrate by intercalating alkali metals such as Li and K, and, in the process, induce electron doping of the sample [9]. Another approach reduces interaction by placing samples over patterned cavities or trenches etched into a supporting substrate [10, 11]. Samples prepared using either of these approaches have shown that suspended MoS_2 samples exhibit altered electronic properties from those of MoS_2 supported directly on the substrate, including a photoluminescence blueshift in the optical gap in freestanding monolayer MoS_2 [12] and a 2- to 10-fold improvement in the carrier mobility in suspended MoS_2 [13].

In this paper, we study the properties and key parameters of suspended monolayer MoS_2 by measuring its electronic structure using micrometer-scale angle-resolved photoemission spectroscopy (micro-ARPES). For comparison, measurements on substrate-supported monolayer MoS_2 were also carried out to provide a baseline case, in which a substrate was present. In addition, the results were independently cross examined using a spectroscopic photoemission-low energy electron microscope (SPELEEM) system. First, our measurements suggest that there is a change in the lattice constant of monolayer MoS_2 *vs.* that in its bulk crystal form. In particular by determining the absolute size of the surface Brillouin zone (SBZ) of monolayer MoS_2, we find a ~3.6% decrease in the SBZ, indicative of a ~3.6% expansion of the in-plane lattice parameter (denoted as **a** in Fig. 1(d)), compared to bulk MoS_2. Second, our results provide insight into the effect of the substrate on the monolayer MoS_2 electronic structure. Due to interactions with the substrate in supported monolayer MoS_2, band structure distortion is observed in comparison to the suspended case. Third, by fitting our measured band dispersions, we extract the effective mass at $\bar{\Gamma}$ and $\bar{K}$ in both suspended and supported monolayer MoS_2.

Our experiments were performed at two synchrotron beamlines. The first was the Spectromicroscopy Beamline at the Elettra Synchrotron light source [14], which provided scanning photoemission microscopy (SPEM) and micro-ARPES measurements of suspended and supported monolayer MoS_2. The spectrometer energy resolution of this instrument was set to 100 meV at a 27 eV incident photon energy and with a beam spot size of 1 μm in diameter. ARPES band structure measurements were also obtained on a SPELEEM system at the National Synchrotron Light Source (NSLS) beam line U5UA [15, 16]. The SPELEEM instrument also allowed imaging by photoemission electron microscopy (PEEM). For both measurements, the samples were annealed in ultra-high vacuum for 2 hours at ~350°C prior to the acquisition of photoemission spectra.

Our crystal samples were exfoliated monolayer MoS_2 flakes, which were examined and calibrated using Raman spectroscopy. To obtain areas of suspended MoS_2, coexisting with supported regions of the flakes, substrates patterned by lithography and etching were used. As schematically shown in Fig. 1(a), a grid pattern of cylindrical cavities with diameters of 2 or 5 μm, and depths of 1 μm were etched into a Si wafer covered with a native oxide; monolayer MoS_2 flakes were then

exfoliated and transferred onto the patterned substrate using the same procedure as described in Ref.[17]. SPEM was used to characterize the sample before investigating the band structure *in-situ* with micro-ARPES. Figures 1(b) & 1(c) show an optical image of an exfoliated monolayer MoS_2 flake before transfer onto the patterned substrate, and the corresponding SPEM image of the partially suspended flake after transfer to the patterned substrate, respectively. Contrast between the suspended MoS_2, supported MoS_2, and the bare substrate is obtained by acquiring locally excited photoelectrons in a kinetic energy window of 18-22 eV, imaged by scanning the sample. Figures 1(e) & 1(f) show an optical image of a MoS_2 flake before transfer, and the corresponding PEEM image of the same flake after transfer to the patterned substrate [18]. Both SPEM and PEEM measurements show clear contrast between suspended and supported MoS_2; thus allowing accurate selection of regions of interest for micro-ARPES measurements in the two different sample regions. Additional experimental details can be found in the Supplemental Material [19].

Figures 2(a)-2(b) show the micro-ARPES band maps of suspended monolayer MoS_2 along the $\bar{\Gamma}$-$\bar{M}$ and $\bar{\Gamma}$-$\bar{K}$ high-symmetry lines of the SBZ, respectively. To better visualize the ARPES features, we perform 2D-curvature processing [20], which is similar to the widely used 1D second-derivative method. The 2D-curvature intensity plot is shown in Figure 2(c). For the micro-ARPES measurements performed at Elettra, the off-normal photon angle-of-incidence uses different selection rules than that of the normal photon angle-of-incidence configuration of the SPELEEM system at U5UA; this difference enabled us to observe the previously invisible S $3p$-derived bands [21]. By measuring beyond the 1st SBZ, we determined the positions of $\bar{K}$ and $\bar{M}$, and found that $\overline{\Gamma K}$ = 1.28±0.04 Å^{-1}, and $\overline{\Gamma M}$ = 1.11±0.04 Å^{-1}, values which are 3.58±3.01% smaller than those of the bulk SBZ ($\overline{\Gamma K}$ = 1.3256 Å^{-1}, $\overline{\Gamma M}$ = 1.1479 Å^{-1}); see Figure 3. While this result is limited by the large error, our measurement suggests the presence of a ~3.6% lateral lattice expansion in monolayer MoS_2 compared to bulk, yielding a lattice constant of 3.28±0.10 Å. In X-ray diffraction and Raman-scattering studies of single layer MoS_2 prepared by exfoliation of Li-intercalated MoS_2 powder immersed in water, Yang *et al.* also reported that the in-plane lattice constant expands to 3.27±0.015 Å, about 3.5% larger than the accepted bulk value (3.16 Å) [22]. The authors attributed this lattice expansion to a change in the Mo coordination from trigonal prismatic for the case of dry MoS_2 to bulk octahedral for the water immersed MoS_2. On a different but related note, there have also been several reports of a blueshift in the in-plane E_{2g}^1 phonon mode of monolayer MoS_2 [23], which has been attributed to reduced interlayer interaction [24]. Our observation of a larger in-plane lattice constant for monolayer Mos_2 would be expected to produce a redshift in the in-plane E_{2g}^1 phonon mode. It thus appears that the reduced interlayer interaction has more of an effect on this phonon mode than our experimentally suggested in-plane lattice constant expansion. We should also note that in our previous SPELEEM measurements, we calibrated the momentum space by assuming that the lattice spacing is unaffected when a MoS_2

crystal is thinned down to a monolayer, i.e., we assumed the same in-plane lattice parameter as for bulk MoS_2 [21].

There are a plethora of density functional theory (DFT) calculations on the band structure of monolayer MoS_2. In addition, there have been several studies of the relaxation of the in-plane lattice constant by way of structural optimization calculations [25-27]. While a thorough theoretical understanding of the full lattice relaxation of MoS_2 is beyond the scope of this experimental paper, we have performed DFT calculations using a range of different out-of-plane lattice constants with the primary purpose of seeking better agreement with our measured electronics structure. In particular, we used the ABINIT code [28, 29], with a generalized gradient approximation (GGA) functional [30]; note that Van der Waals interactions are not pertinent for calculation of our experimentally realized suspended monolayer MoS_2 crystal. These calculations investigated the corresponding modification of the intraplane distance (denoted as **z** in Fig. 1(b)) between the Mo and S atomic planes while utilizing the experimentally determined in-plane lattice constant stated above. Our result shows that when **z** is allowed to increase by ~2% compared to its bulk value (z=1.586Å) [31], the calculated bands agree surprisingly closely with the experimental measurements [19], even though our calculation does not capture many of the detailed physics of our crystal, such as spin-orbit coupling [25]. Note that our suggested increase in **z** is in contrast to a low-energy-electron-diffraction study of the top layer of single-crystal bulk MoS_2, which reported a ~5% decrease of **z** within the topmost layer [32]. We again note that our deduction of an expansion of the out-of-plane lattice constant is driven simply by a desire to seek better agreement of the DFT-derived bands with measurements and is not a definitive finding.

The intrinsic nature of the experimentally suggested increase in the in-plane monolayer lattice constant is supported by our micro-ARPES measurements of supported monolayer MoS_2, from which an approximately identical relaxed lattice constant, within our error, is extracted (a=3.30±0.10Å, see Supplemental Material [19]). Figures 2(d)-2(e) show the ARPES band maps of supported monolayer MoS_2 along the $\bar{\Gamma}$-$\bar{M}$ and $\bar{\Gamma}$-$\bar{K}$ high-symmetry lines of the SBZ, respectively. Figure 2(f) is the corresponding 2D-curvature intensity plot [20]. Our calculated bands (using the relaxed lattice parameters) are overlaid onto Fig. 2(a)-2(f) for comparison. Note that Fig. 2(a)-2(b) & 2(d)-2(e) are all normalized to the highest intensity of their respective band maps.

Note that, as shown in Fig. 2 (e)&(f), the valence band maximum at $\bar{K}$ is still higher than that at $\bar{\Gamma}$, which means that the relaxation of the lattice constant for monolayer MoS_2 does not alter the location of the valence band maximum in the BZ. This result indicates that the key conclusion in our previous work [21], i.e., the valence band maximum shift from $\bar{\Gamma}$ to $\bar{K}$, when MoS_2 is thinned down to 1ML, remains intact.

In our previous study, we had also tentatively attributed a "compression" in the measured dispersion of the UVB, relative to the DFT derived UVB, to surface

interaction. The present work, which measures both supported and suspended monolayer MoS_2, suggests, on the other hand, that the compression is predominately due to lattice relaxation. While surface interactions are present, we deduce them to be relatively weak, due to the fact that electronic structure of the substrate-supported monolayer MoS_2 does not differ significantly from that of the suspended case.

Figure 4(a) shows the UVB of suspended monolayer MoS_2 and Fig. 4(b)-4(c) along with the corresponding energy distribution curves (EDCs). Our measurements of suspended MoS_2 that are free from substrate interaction, and the access to precise absolute parallel momentum values afforded by the spectromicroscopy instrumentation, enable us to fully investigate the effective mass (m_{eff}) of intrinsic MoS_2. Note that effective mass is a particularly important parameter in transport measurements since it plays a crucial role in determining the sample mobility. Despite many theoretical predictions of the effective mass of monolayer MoS_2, there remains a glaring lack of agreement. Further transport measurements of the effective mass have thus far been lacking. Table I summarizes several predicted values of the effective mass reported by different theoretical groups using different DFT techniques/functionals [7, 27, 33-35]. The simplest approach to fitting the data uses a parabolic fitting over a range of $\pm 0.08 Å^{-1}$; we extract the effective mass at $\bar{\Gamma}$ and $\bar{K}$ to be $(2.00\pm0.35)m_0$ and $(0.43\pm0.02)m_0$, respectively. The value at $\bar{K}$ agrees most closely with the value reported by Kormányos et $al.$, while the value at $\bar{\Gamma}$ is very close to the value reported by Cheiwchanchamnangij et al.

In the substrate-supported case, we extract values of the hole effective mass that are not too different from that of intrinsic, i.e., suspended MoS_2. We find values of m_{eff} at $\bar{\Gamma}$ and $\bar{K}$ of $(1.85\pm0.22)m_0$ and $(0.48\pm0.02)m_0$, respectively. We note that the effective mass value stated here is somewhat lower than that quoted in our previous work [21]. We attribute that difference to the improved energy resolution and better signal to noise available using the SPEM; also, the inverse relation between dispersion and effective mass accentuates small differences in the relatively flat dispersion around $\bar{\Gamma}$.

At $\bar{K}$ in crystal momentum space, the UVB of monolayer MoS_2 is derived primarily from the Mo $d_{x^2-y^2}/d_{xy}$ orbitals [36]. Due to broken inversion symmetry and strong spin-orbit coupling, a spin-splitting of 148 meV at $\bar{K}$ has been predicted by theory [25]. This splitting in the upper valence band has been of recent interest for exploration of the coupling of spin and valley degree of freedom in MoS_2 [37]. Since we were not able to directly resolve this spin-orbit splitting in our ARPES measurements, we did examine carefully the variation of the linewidth of the upper-most valence band with change in crystal momentum, and observe the following. We performed single Gaussian peak fitting (with a linear background) to the EDCs of the upper-most valence band to extract the FWHM of the Gaussian peak. The linewidth vs momentum plot is shown in Fig. 4 (d). Using the blue dashed line as a guide to the eye, we find that the EDC linewidth remains constant with a small

variation (450±19 meV) from $\bar{M}$ to the midpoint (defined as $\bar{A}$) of $\overline{\Gamma K}$. Note that the relatively bigger error bars in the vicinity of $k_{||}$ = -0.5Å^{-1} is due to the vanishing spectrum intensity. In the vicinity of the midpoint of $\overline{\Gamma K}$, which is enclosed by a black dashed box in Fig. 4 (a) & (d), the linewidth gradually increases. In the vicinity of $\bar{K}$, the linewidth (528±13 meV) is found to be larger than that at $\bar{M}$ and $\bar{\Gamma}$.

Regarding the origin of this increased linewidth, we make the following observation. There are two possible explanations for this sharp linewidth increase in the vicinity of $\bar{A}$ to $\bar{K}$: 1) a decrease in the quasi-particle lifetime or 2) a splitting of the spin degenerate band into two bands due to spin-orbit coupling. We favor the latter explanation due to the location being consistent with theoretical calculations of the splitting in MoS$_2$. However it is clear that a definitive conclusion of this linewidth increase awaits higher resolution studies.

In conclusion, we have performed ARPES measurements on the valence bands of suspended and supported monolayer MoS$_2$. Our ARPES measurements of suspended MoS$_2$ reveal good qualitative and quantitative agreement with theory and elucidate the effects of a native-oxide covered Si substrate on the band structure of monolayer MoS$_2$. We find a suggested expansion of the in-plane lattice constant and deduce an expansion of the intraplane lattice constant, which may be indicative of an atomic structure that is sensitive to stacking. Fitting of the measured valence band dispersion provides an experimentally derived value for the effective mass of both suspended and substrate-supported monolayer MoS$_2$. We also measure an increase in the linewidth over the band region from the midpoint of $\overline{\Gamma K}$ to the vicinity of $\overline{K}$.

* Email: osgood@columbia.edu

References

[1] B. Radisavljevic, A. Radenovic, J. Brivio, V. Giacometti, and A. Kis, Nature nanotechnology **6**, 147 (2011).
[2] D. Lembke, and A. Kis, ACS nano **6**, 10070 (2012).
[3] K. F. Mak, C. Lee, J. Hone, J. Shan, and T. F. Heinz, Phys. Rev. Lett. **105**, 136805 (2010).
[4] S. Zhou, G.-H. Gweon, A. Fedorov, P. First, W. De Heer, D.-H. Lee, F. Guinea, A. C. Neto, and A. Lanzara, Nature materials **6**, 770 (2007).
[5] J.-H. Chen, C. Jang, S. Xiao, M. Ishigami, and M. S. Fuhrer, Nature nanotechnology **3**, 206 (2008).
[6] C. Dean, A. Young, I. Meric, C. Lee, L. Wang, S. Sorgenfrei, K. Watanabe, T. Taniguchi, P. Kim, and K. Shepard, Nature nanotechnology **5**, 722 (2010).
[7] T. Cheiwchanchamnangij, and W. R. Lambrecht, Physical Review B **85**, 205302 (2012).
[8] A. Molina-Sanchez, and L. Wirtz, Physical Review B **84**, 155413 (2011).
[9] G. Eda, H. Yamaguchi, D. Voiry, T. Fujita, M. Chen, and M. Chhowalla, Nano letters **11**, 5111 (2011).
[10] A. Locatelli, K. R. Knox, D. Cvetko, T. O. Mentes, M. A. Nino, S. Wang, M. B. Yilmaz, P. Kim, R. M. Osgood Jr, and A. Morgante, ACS nano **4**, 4879 (2010).
[11] K. R. Knox, A. Locatelli, M. B. Yilmaz, D. Cvetko, T. O. Menteş, M. Á. Niño, P. Kim, A. Morgante, and R. M. Osgood Jr, Physical Review B **84**, 115401 (2011).
[12] N. Scheuschner, O. Ochedowski, A.-M. Kaulitz, R. Gillen, M. Schleberger, and J. Maultzsch, Physical Review B **89**, 125406 (2014).
[13] T. Jin, J. Kang, E. S. Kim, S. Lee, and C. Lee, Journal of Applied Physics **114**, 164509 (2013).
[14] P. Dudin, P. Lacovig, C. Fava, E. Nicolini, A. Bianco, G. Cautero, and A. Barinov, Journal of Synchrotron Radiation **17**, 445 (2010).
[15] J. I. Flege, E. Vescovo, G. Nintzel, L. H. Lewis, S. Hulbert, and P. Sutter, Nucl. Instrum. Meth. B **261**, 855 (2007).
[16] P. Sutter, M. Hybertsen, J. Sadowski, and E. Sutter, Nano Lett. **9**, 2654 (2009).
[17] P.-C. Yeh, W. Jin, N. Zaki, D. Zhang, J. T. Sadowski, A. Al-Mahboob, A. M. van der Zande, D. A. Chenet, J. I. Dadap, and I. P. Herman, Physical Review B **89**, 155408 (2014).
[18] E. Bauer, M. Mundschau, W. Swiech, and W. Telieps, Ultramicroscopy **31**, 49 (1989).
[19] See Supplemental Material at URL for more details about experiment procedure, PEEM image, and lattice constant expansion.
[20] P. Zhang, P. Richard, T. Qian, Y. M. Xu, X. Dai, and H. Ding, Rev. Sci. Instrum. **82**, 043712 (2011).
[21] W. Jin, P.-C. Yeh, N. Zaki, D. Zhang, J. T. Sadowski, A. Al-Mahboob, A. M. van der Zande, D. A. Chenet, J. I. Dadap, and I. P. Herman, Physical Review Letters **111**, 106801 (2013).
[22] D. Yang, S. J. Sandoval, W. Divigalpitiya, J. Irwin, and R. Frindt, Physical Review B **43**, 12053 (1991).

[23]   C. Lee, H. Yan, L. E. Brus, T. F. Heinz, J. Hone, and S. Ryu, Acs Nano **4**, 2695 (2010).

[24]   X. Luo, Y. Zhao, J. Zhang, Q. Xiong, and S. Y. Quek, Physical Review B **88**, 075320 (2013).

[25]   Z. Zhu, Y. Cheng, and U. Schwingenschlögl, Phys. Rev. B **84**, 153402 (2011).

[26]   A. Ramasubramaniam, Phys. Rev. B **86**, 115409 (2012).

[27]   W. S. Yun, S. W. Han, S. C. Hong, I. G. Kim, and J. D. Lee, Phys. Rev. B **85**, 033305 (2012).

[28]   X. Gonze, Zeitschrift für Kristallographie - Crystalline Materials **220**, 558 (2005).

[29]   X. Gonze, B. Amadon, P.-M. Anglade, J.-M. Beuken, F. Bottin, P. Boulanger, F. Bruneval, D. Caliste, R. Caracas, and M. Cote, Comput. Phys. Commun. **180**, 2582 (2009).

[30]   J. P. Perdew, K. Burke, and M. Ernzerhof, Physical Review Letters **77**, 3865 (1996).

[31]   T. Böker, R. Severin, A. Müller, C. Janowitz, R. Manzke, D. Voß, P. Krüger, A. Mazur, and J. Pollmann, Phys. Rev. B **64**, 235305 (2001).

[32]   B. Mrstik, R. Kaplan, T. Reinecke, M. Van Hove, and S. Tong, Physical Review B **15**, 897 (1977).

[33]   H. Peelaers, and C. G. Van de Walle, Phys. Rev. B **86**, 241401 (2012).

[34]   A. Kormányos, V. Zólyomi, N. D. Drummond, P. Rakyta, G. Burkard, and V. I. Fal'ko, Physical Review B **88**, 045416 (2013).

[35]   A. Kormányos, V. Zólyomi, N. D. Drummond, and G. Burkard, Physical Review X **4**, 011034 (2014).

[36]   E. Cappelluti, R. Roldán, J. Silva-Guillén, P. Ordejón, and F. Guinea, Physical Review B **88**, 075409 (2013).

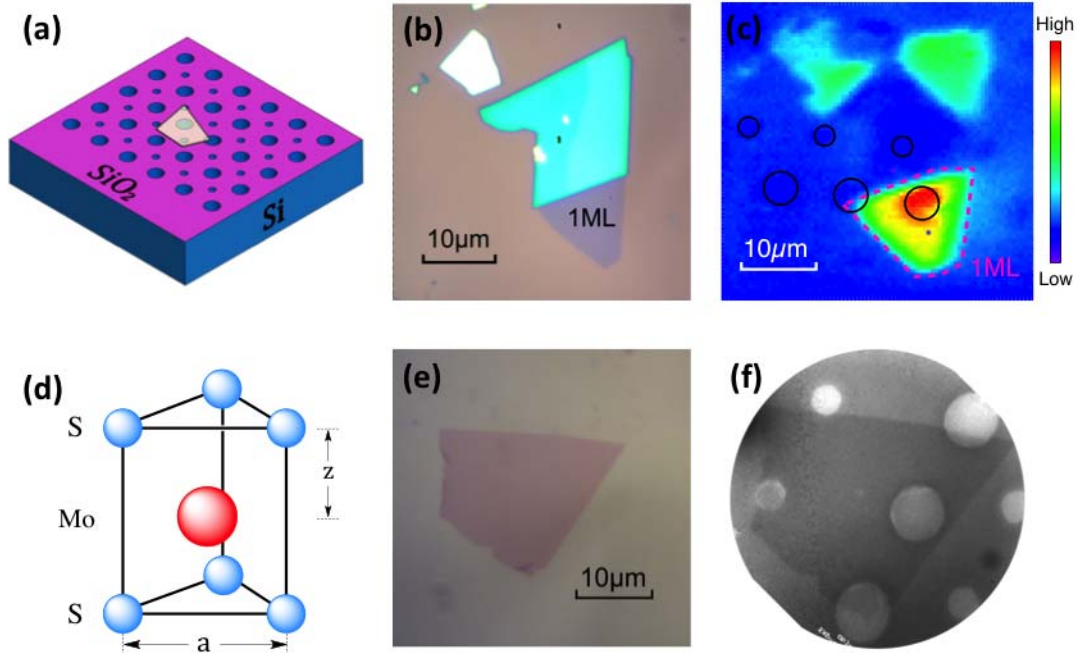[37]   K. F. Mak, K. He, J. Shan, and T. F. Heinz, Nat Nano **7**, 494 (2012).

Fig. 1. (a) Sketch of the sample configuration. Monolayer MoS_2 flakes were transferred onto patterned silicon chips (blue) with native oxide (purple). (d) Atomic structure of monolayer MoS_2. The in-plane lattice constant is denoted as **a**, and the interplane distance between Mo and S atomic planes in the same 'monolayer' sheet is denoted as **z**. (b) & (e) Optical microscope images of the exfoliated monolayer MoS_2 samples. (c) Scanning photoemission microscopy map corresponding to the sample shown in panel (b), acquired with photon energy of 27 eV by collecting photoelectrons with an energy window of 18-22 eV. The area of monolayer MoS_2 flake is enclosed by a dashed pink frame, and the suspended regions are marked with black circles. (f) PEEM image of sample shown in panel (e).
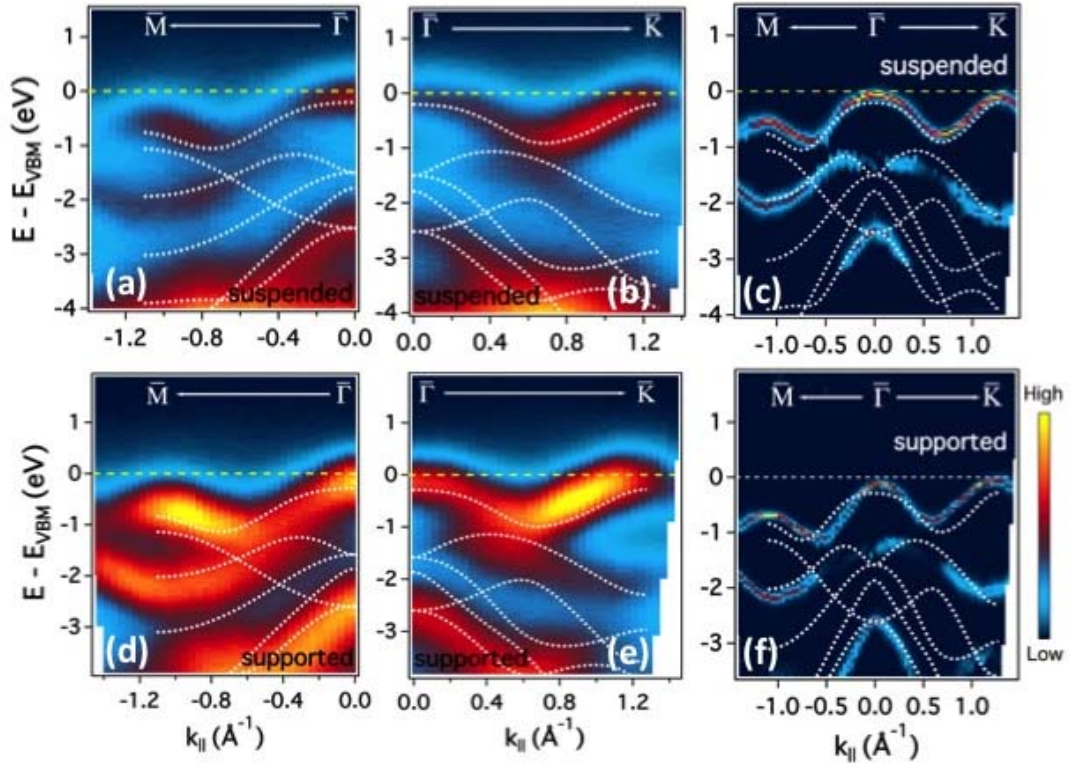
Fig. 2. (a)-(b) Micro-ARPES band maps of suspended MoS₂ along $\bar{\Gamma} - \bar{M}$ and $\bar{\Gamma} - \bar{K}$, respectively. (c) 2D-curvature intensity plot of the suspended MoS₂ bands along $\bar{M} - \bar{\Gamma} - \bar{K}$ high symmetry line. (d)-(e) ARPES band maps of supported MoS₂ along $\bar{\Gamma} - \bar{M}$ and $\bar{\Gamma} - \bar{K}$, respectively. (f) 2D-curvature intensity plot of the supported MoS₂ bands along $\bar{M} - \bar{\Gamma} - \bar{K}$ high symmetry line. DFT-calculated bands using the relaxed lattice parameters are overlaid onto all the band maps for comparison.
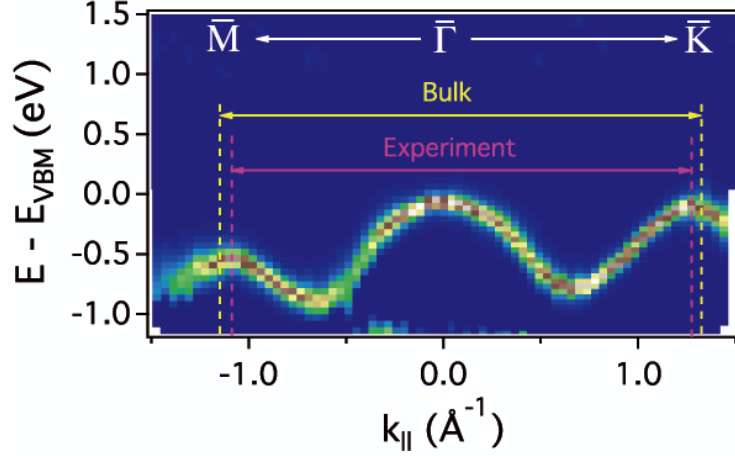
Fig. 3. 2D curvature plot of the uppermost valence band (UVB) of suspended monolayer MoS_2 along high symmetric direction. Pink dashed lines mark the local maximum of the UVB extracted from ARPES measurement and the yellow dashed lines denote the positions of   and   using the lattice constant of bulk MoS_2.

TABLE I: Effective mass extracted from DFT calculation (Ref. [7, 27, 33-35]) and ARPES measurements.

	Package/functional		
S.W. Yun *et al*	FLAPW/GGA	3.524	0.637
Andor Kormányos *et al*	VASP/HSE06	2.24	0.53
H. Peelaers *et al*	VASP/HSE06	2.8	0.44
T. Cheiwchanchamnangij *et al*	Quasiparticle GW/LDA	3.108	0.428
Experiment on suspended MoS_2	N/A	2.00	0.43
Experiment on supported MoS_2	N/A	1.85	0.48
This work (without spin-orbit interaction)	ABINIT/ GGA	2.65	0.52
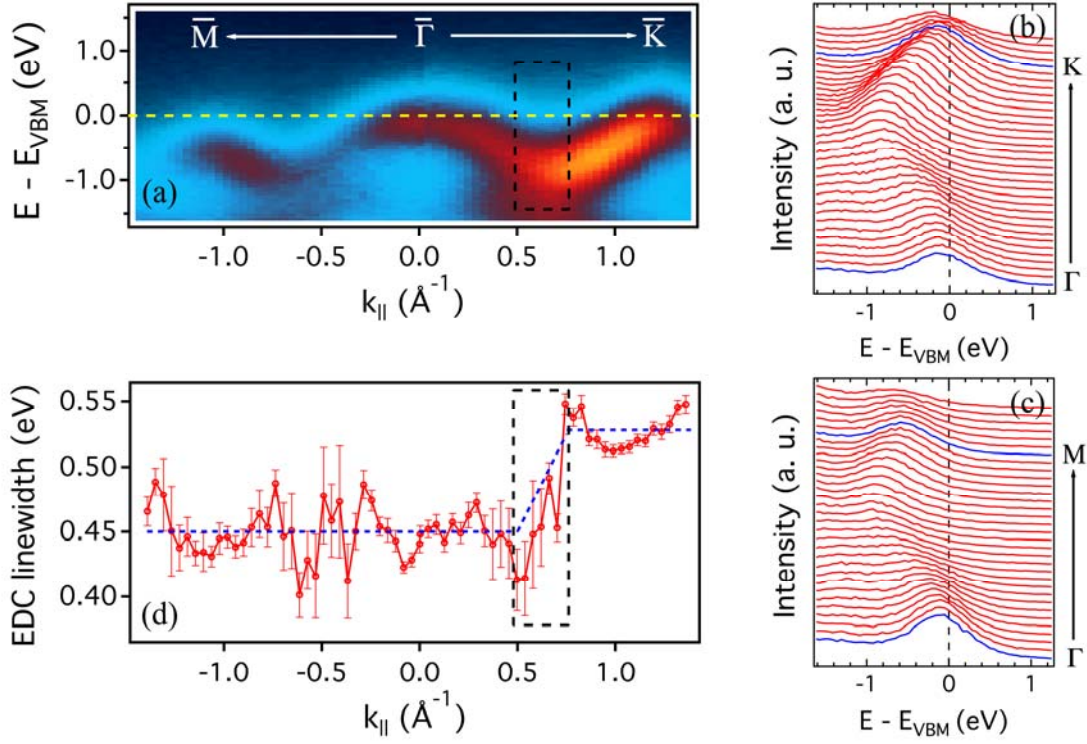
Fig. 4. (a) UVB of suspended monolayer MoS₂. (b)-(c) EDCs of the UVB along the $\overline{\Gamma}$-$\overline{K}$ and $\overline{\Gamma}$-$\overline{M}$ direction, respectively. (d) Gaussian linewidth *vs* momentum plot. The blue dashed lines are the guide to the eyes to trace the evolution of the linewidth with momentum. The black dashed boxes in (a) & (d) enclose the transition region where the linewidth increases.